

## **EFFECT OF BODY SHAPE ON THE AERODYNAMICS OF PROJECTILES AT SUPERSONIC SPEEDS**

ABDULKAREEM SH. MAHDI AL-OBAIDI\*, MUSHTAK AL-ATABI

School of Engineering, Taylor's University College, No 1 Jalan SS 15/8  
47500 Subang Jaya, Selangor DE, Malaysia.

\*Corresponding Author: [abdulkareem.mahdi@taylors.edu.my](mailto:abdulkareem.mahdi@taylors.edu.my)

### **Abstract**

An investigation has been made to predict the effects of forebody and afterbody shapes on the aerodynamic characteristics of several projectile bodies at supersonic speeds using analytical methods combined with semi-empirical design curves. The considered projectile bodies had a length-to-diameter ratio of 6.67 and included three variations of forebody shape and three variations of afterbody shape. The results, which are verified by comparison with available experimental data, indicated that the lowest drag was achieved with a cone-cylinder at the considered Mach number range. It is also shown that the drag can be reduced by boattailing the afterbody. The centre-of-pressure assumed a slightly rearward location for the ogive-cylinder configuration when compared to the configuration with boattailed afterbody where it was the most forward. With the exception of the boattailed afterbody, all the bodies indicated inherent static stability above Mach number 2 for a centre-of-gravity location at about 40% from the body nose.

Keywords: Projectile, Forebody and Afterbody, Supersonic speed, Aerodynamics.

### **1. Introduction**

The shape of a projectile is generally selected on the basis of combined aerodynamic, guidance, and structural considerations. The choice of seeker, warhead, launcher, and propulsion system has a large impact on aerodynamic design [1]. Consequently, various configurations have evolved, each resulting from a series of design compromises. During supersonic flight, the drag component that results from the change of the cross section of the projectile is referred to as wave drag and it is attributed to the shock waves formed. This normally happens at the forebody (nose) and afterbody (tail). Since the wave drag may be the prevailing drag form at supersonic speeds, careful selection of the

**Nomenclatures**

$C_{BT}$	Boattail factor
$C_{Cyl}$	Contribution of cylindrical afterbody part on the centre-of-pressure coefficient of the nose
$C_D$	Drag force coefficient
$C_{D_0}$	Zero-lift drag coefficient
$C_N$	Normal force coefficient
$C_{N_\alpha}$	Normal-force-curve slope, 1/rad
$C_l$	Theoretical normal force slope parameter, 1/rad
$(c_p)_{BT}$	Boattail centre-of-pressure coefficient
$D_o$	Ratio of diameter of nose blunting to cylinder diameter ( $2r_o/d$ )
$d$	Body diameter, m
$d_{BT}$	Boat-tail diameter, m
$K_b$	Correction factor for base drag
$L$	Projectile body length, m
$L_N$	Nose length, m
$L'_N$	Original nose length of pointed conical nose (Fig. 1), m
$L_{ref}$	Reference length ( $d$ ), m
$M$	Freestream Mach number
$p_b$	Base pressure coefficient for cylindrical boattail
Re	Reynolds number
$r_o$	Radius of nose blunting (Fig. 1), m
$S_{ref}$	Reference area ( $\pi d^2/4$ ), m <sup>2</sup>
$S_{wet}$	Body wetted area (base area is not included), m <sup>2</sup>
$x_{cg}$	Centre-of-gravity location measured from the nose apex, m
$x_{cp}$	Centre-of-pressure location measured from the nose apex, m

**Greek Symbols**

$\alpha$	Angle of attack, deg.
$\beta$	Mach number parameter, $\sqrt{M^2 - 1}$
$\eta_{BT}$	Ratio of base diameter to cylinder diameter ( $d_{BT}/d$ )
$\eta_{Cyl}$	Ratio of cylindrical part length to nose length ( $L_{Cyl}/L_N$ )
$\eta'_{Cyl}$	Ratio of cylindrical part length to nose length of pointed cone shape
$\eta_o$	Correction factor for nose bluntness
$\lambda_{BT}$	Boattail fineness ratio ( $L_{BT}/d$ )
$\lambda_{Cyl}$	Ratio of cylindrical part length to diameter ( $L_{Cyl}/d$ )
$\lambda_N$	Nose fineness ratio ( $L_N/d$ )
$\lambda'_N$	Fineness ratio of original pointed cone ( $L'_N / d$ )
$\theta$	Semi-vertex angle of the conical nose (Fig. 1), deg.

nose and tail shapes is mandatory to ensure performance and operation of the over-all system.

Shahbhang and Rao [2] conducted an experimental investigation to determine aerodynamic characteristics of cone-cylinder and ogive-cylinder bodies of different fineness ratios at Mach number of 1.8. Their results indicated that the

normal force for ogive-cylinder body is slightly higher than that for cone-cylinder body of nose fineness ratio 3 and lower than that for cone-cylinder body for nose fineness ratio 7 and there is crossing of normal force curves for nose fineness ratio equal to 5. This interesting phenomenon requires further investigation.

Clement and deMoraes [3] presented results of a free-flight investigation at supersonic speeds to determine zero-lift drag of a series of bodies of revolution. They showed that for supersonic speeds, parabolic bodies exhibit 9 to 18 percent less drag compared to  $8^\circ$  cone-cylinder bodies having the same volume and maximum diameter.

Cohen [4] experimentally investigated the aerodynamic characteristics of four slender pointed-nose bodies of revolution of fineness ratios 12.2 and 14.2 at freestream Mach numbers of 1.50, 1.60, 1.79, and 1.99 through a range of angles of attack ( $0^\circ$  to  $10^\circ$ ). At angle of attack of  $0^\circ$ , boattailing increased the model fore drag but decreased the measured base drag appreciably with a resultant decrease of total drag. Also the decreasing of boattail convergence increased the measured base drag but reduced the model fore drag with a resultant decrease of the model total drag.

The objectives of this paper is to predict the aerodynamic characteristics of projectiles using analytical and semi-empirical methods and study the effect of body shape; forebody and afterbody, on the aerodynamic characteristics of projectiles at supersonic speeds. For this purpose five widely used projectile shapes are investigated. The geometry and full dimensions of these projectile shapes are shown in Fig. 1. The models are: (a) cone-cylinder, (b) ogive-cylinder, (c) blunted cone-cylinder, (d) cone-cylinder boattail ( $4^\circ$ ), and (e) cone-cylinder boattail ( $8^\circ$ ). All the models have a fineness ratio of 6.67 and a centre-of-gravity location at about the 40% body station. The supersonic Mach number range considered is from 1.6 to 5 for zero-angle of attack.

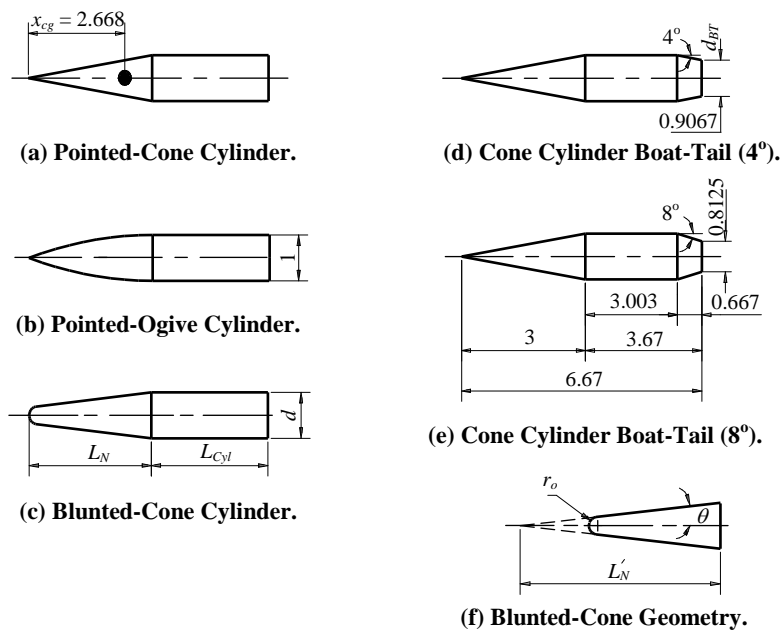


Fig. 1. Investigated Shapes of Projectiles (Geometry and Dimensions).

## 2. Prediction of Aerodynamic Coefficients

Analytical methods and design charts used for the prediction of zero-lift drag coefficient  $C_{D0}$ , normal-force-curve slope  $C_{N\alpha}$ , and centre-of-pressure location  $x_{cp}$  of body of revolution at supersonic speeds are presented in this section. The analytical methods are based on supersonic linearised theory and thus they are limited to slender bodies and low angles of attack, i.e. in the linear range of the normal-force-curve slope while the design charts are produced from semi-empirical results. The design charts are coupled with the analytical methods to improve the accuracy of the results. These design charts used for the prediction of aerodynamics characteristics are adapted from Ref. [5] and [6] and converted to numerical data, as outlined in *Appendix A*.

### 2.1. Zero-lift drag coefficient $C_{D0}$

The total zero-lift drag coefficient of the body is usually considered to be of three components; friction drag, wave drag, and base drag as shown in Eq. (1). These different components are further discussed in the following sub-sections.

$$C_{D0} = C_{D_f} + C_{D_w} + C_{D_b} \quad (1)$$

#### 2.1.1. Friction drag coefficient

For fully-turbulent and compressible flow, the friction coefficient is given by Eq. (2) [7 and 8]

$$C_{D_f} = \frac{0.455(\log_{10} \text{Re})^{-2.58} S_{wet}}{(1 + 0.21M^2)^{0.467} S_{ref}} \quad (2)$$

#### 2.1.2. Wave drag coefficient

The main contribution to the wave drag arises from nose and afterbody. The magnitude of the wave drag depends primarily on the Mach number, the shape and dimensions of the nose or afterbody. Therefore, the total wave drag of the body is simply the summation of the nose and afterbody wave drags

$$C_{D_w} = (C_{D_w})_N + (C_{D_w})_{BT} \quad (3)$$

The wave drag of pointed cone-cylinder  $(C_{D_w})_{cone}$  and pointed ogive-cylinder  $(C_{D_w})_{ogive}$  can be obtained from Figs. A-1 and A-2 (*Appendix A*) as a function of nose fineness ratio  $\lambda_N$ , and Mach number. For blunted cone-cylinder the wave drag can be determined as a function of  $\lambda_N$ , Mach number, and diameter of nose bluntness  $D_0$  using Eq. (4) [6]

$$(C_{D_w})_{bluntedcone} = (C_{D_w})_{cone}(1 - D_0^2 \cos^2 \theta) + (C_{D_w})_{sphere} D_0^2 \quad (4)$$

where  $(C_{D_w})_{cone}$  is the wave drag of the original pointed cone with  $\lambda'_N = 0.5/\tan\theta$ , and  $(C_{D_w})_{sphere}$  is the wave drag of hemispherical nose, which can be determined from Fig. A-3 as function of  $\lambda_N$  and Mach number.

The wave drag of conical boattail  $(C_{D_w})_{BT}$  can be evaluated from Fig. A-4 as a function of  $\lambda_{BT}$ ,  $\eta_{BT}$  and Mach number.

### 2.1.3. Base drag coefficient

At supersonic speeds the base drag of the body, caused by a large negative pressure, results in a substantial increase in the body drag. The base drag coefficient of the body is related to the base pressure coefficient as follows [6]

$$C_{D_b} = -p_b K_b \eta_{BT}^2 \quad (5)$$

where  $p_b$  is the base pressure coefficient for cylindrical base (determined from Fig. A-5 as a function of Mach number), and  $K_b$  is a correction factor, which depends on the geometry of boattail  $K_b = f(C_{BT}, M)$ , obtained from Fig. A-6 [6], where

$$C_{BT} = \frac{1 - \eta_{BT}}{2\lambda_{BT}\eta_{BT}^2} \quad (6)$$

## 2.2. Normal-force-curve slope $C_{N\alpha}$

The total normal-force-curve slope of nose-cylinder-boattail body is determined by the summation of the normal-force-curve slopes of the nose (with the effect of cylindrical part) and afterbody.

$$C_{N\alpha} = (C_{N\alpha})_N + (C_{N\alpha})_{BT} \quad (7)$$

At supersonic speeds design charts are presented for estimating the normal-force-curve slope of bodies of revolution composed of conical or ogival noses and cylindrical afterbodies.

Figs. A-7 and A-8 present  $(C_{N\alpha})_{N\Box}$  based on the body cross section area for bodies with conical  $(C_{N\alpha\Box})_{cone}$  and ogival  $(C_{N\alpha\Box})_{ogive}$  noses respectively, where the effect of cylindrical part aft nose is taken into consideration.

The normal-force-curve slope of blunted cone-cylinder can be evaluated from [5] as a function of  $\lambda_N$ , Mach number, and  $D_0$

$$(C_{N\alpha})_N = (C_{N\alpha})_{cone} (1 - D_0^2) + (C_{N\alpha})_{sphere} D_0^2 \quad (8)$$

where  $(C_{N\alpha})_{cone}$  is the normal-force-curve slope of pointed cone with  $\beta/\lambda'_N$  and  $\eta'_{Cyl}$ , and  $(C_{N\alpha})_{sphere}$  is the normal-force-curve slope of hemispherical nose, which can be determined from Fig. A-9 as function of  $\beta/\lambda_{Cyl}$ .

The normal-force-curve slope of conical boattail depends on the dimensions of the afterbody and Mach number. It is determined as follows [6]

$$(C_{N\alpha})_{BT} = (C_1)_{BT} (1 - \eta_{BT}^2) \quad (9)$$

where  $(C_1)_{BT}$  can be determined from Fig. A-10 as a function of  $\beta/\lambda_{BT}$ .

## 2.3. Location of the centre-of-pressure $x_{cp}$

The identification of the location of the centre of pressure of a projectile body is motivated by the need for calculating aerodynamic moments, stability and structural analyses. The centre-of-pressure location of bodies composed of conical noses and cylindrical afterbodies is determined as follows [7]

$$(x_{cp})_N = (0.667 + C_{Cyl})L_N \quad (10)$$

and for bodies with ogival noses

$$(x_{cp})_N = (0.467 + C_{Cyl})L_N \quad (11)$$

where  $C_{Cyl}$ , the contribution of cylindrical afterbody part on the centre-of-pressure coefficient of the nose, is obtained from Fig. A-11 as a function of  $\beta/\lambda_N$  and  $1/\lambda_{Cyl}$ .

For bodies with blunted cone-cylinder, the bluntness of the nose is introduced by the correction factor  $\eta_0$

$$(x_{cp})_N = (0.667\eta_0 + C_{Cyl})L_N \quad (12)$$

The factor  $\eta_0$  is obtained from Fig. A-12 as a function of  $D_0$ .

The centre-of-pressure location of boattail measured from the nose apex is given by

$$(x_{cp})_{BT} = L_N + L_{cyl} + (c_p)_{BT} L_{BT} \quad (13)$$

where  $(c_p)_{BT}$  is determined from Fig. A-13 as a function of  $\beta/\lambda_{BT}$ .

The overall centre-of-pressure location of the body measured from the nose apex is given by

$$x_{cp} = \frac{(x_{cp})_N (C_{N_a})_N + (x_{cp})_{BT} (C_{N_a})_{BT}}{C_{N_a}} \quad (14)$$

### 3. Computer Programme: Validation and Verification

For the purposes of prediction and analysis of aerodynamic characteristics, a computer programme is developed. The restrictions, capabilities, and the flow charts of the programme are given in *Appendix B*.

To ensure the validity and accuracy of the calculations, the results are compared to available experimental wind tunnel data. Normal force coefficient and base drag coefficient are compared as a function of Mach number and angle of attack. Two typical projectile configurations (as shown in Figs. 2 and 3) are selected for this purpose. The specifications of the models and test conditions are shown in Table 1.

**Table 1. Test Model Specifications and Test Conditions.**

	Model No. 1 [2]	Model No. 2 [4]
<b>Configuration Type</b>	Cone-cylinder	Ogive-cylinder
<b>Body fineness ratio</b>	13	12.2
<b>Nose fineness ratio</b>	3	7.5
<b>Body Diameter, <math>d</math> (inches)</b>	1	6
<b>Reference length, <math>L_{ref}</math></b>	$d$	$d$
<b>Reference area, <math>S_{ref}</math></b>	$\pi d^2/4$	$\pi d^2/4$
<b>Testing Mach number</b>	1.77	1.5, 1.6, 1.79, 1.99
<b>Testing angle of attack (deg.)</b>	0 – 6	0

Figures 2 and 3 show the comparison between the current results and the wind tunnel experimental data. Fig. 2 shows that at low angles of attack the normal force coefficients are in excellent agreement with the experimental data. This is to be expected due to the assumption of small angle of attack. The figure also shows that the current results are closer (average percentage error less than 0.5%) to the experimental data than those predicted analytically (average percentage error about 6%) by Shahbahang and Rao [2]. This is expected as the analytical methods contained a number of simplifying assumptions that limit their accuracy and range of use.

A comparison of base drag coefficient as a function of Mach number is shown in Fig. 3. The comparison shows that at low supersonic Mach numbers the average percentage error is 12%, while at higher Mach number the accuracy is excellent (error less than 2%). At low supersonic Mach numbers the base drag contribution is greater than the wave drag of nose, but with increasing Mach number the wave drag contribution is the largest [9]. However the obtained accuracy is still within the range of 10% error, which is considered sufficient to be used in the preliminary design of projectiles and missiles [10].

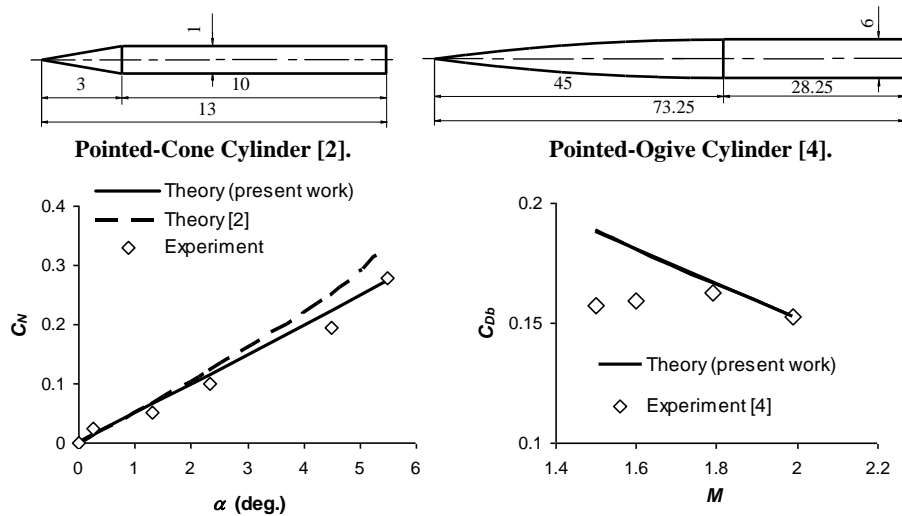


**Fig. 2. Variation of Normal Force vs. Angle of Attack at  $M = 1.77$ .**

**Fig. 3. Variation of Base Drag Coefficient vs. Mach Number**

## 4. Results and Discussion

The prediction of the aerodynamic coefficients of the investigated projectiles shown in Fig. 1 was carried using the methods and the computer programme described above. The effects of forebody and afterbody shapes on the aerodynamics at supersonic speeds are analysed in this paper.

### 4.1. Effect of forebody

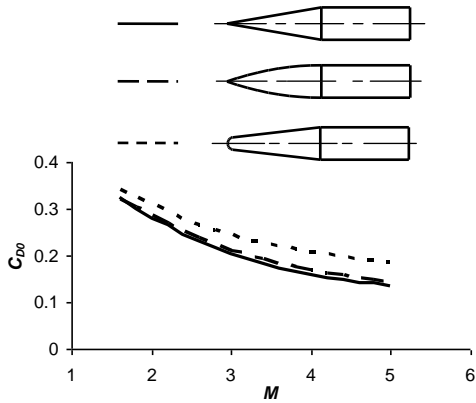
#### Zero-lift drag $C_{D0}$

Figure 4(a) shows the effect of nose shape on  $C_{D0}$  with cylindrical afterbody as a function of Mach number. The drag of cone-cylinder combination was the lowest

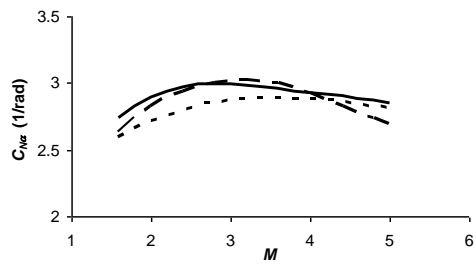
at the considered Mach numbers. It is clear that the bluntness of nose causes the drag to increase.

**Normal-force-curve-slope  $C_{N\alpha}$  and location of centre-of-pressure  $x_{cp}$**

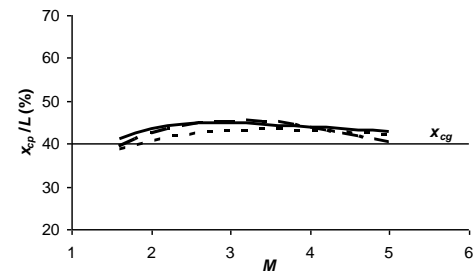
The effect of forebody on the normal force curve slope and centre-of-pressure location for the cylindrical afterbody is shown in Figs. 4(b) and (c) as a function of Mach number. For all three shapes the variations of  $x_{cp}$  are reasonably similar and in general indicate the most rearward location with the ogival nose. The centre-of-pressure locations are apparently a result of the normal force distribution over the bodies with the blunted cone producing the least lift forward, thus resulting in a more rearward  $x_{cp}$ .



(a) Zero-Lift Drag Coefficient  $C_{D0}$ .

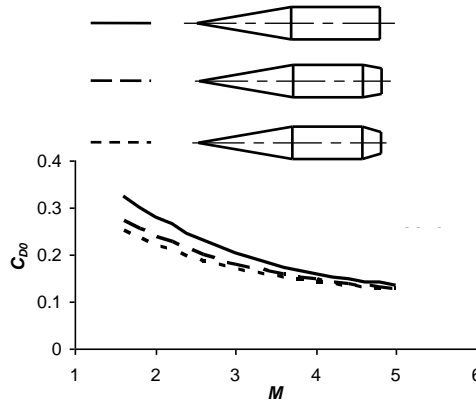


(b) Normal-Force-Curve Slope  $C_{N\alpha}$ .

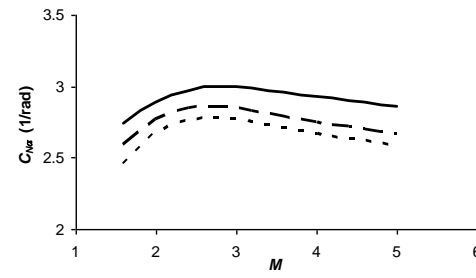


(c) Centre-of-Pressure Location  $x_{cp}/L$ .

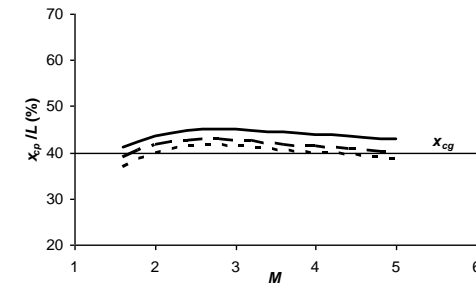
**Fig. 4. Effect of Forebody Shape on the Aerodynamic Characteristics.**



(a) Zero-Lift Drag Coefficient  $C_{D0}$ .



(b) Normal-Force-Curve Slope  $C_{N\alpha}$ .



(c) Centre-of-Pressure Location  $x_{cp}/L$ .

**Fig. 5. Effect of Afterbody Shape on the Aerodynamic Characteristics.**

For conical, ogival, and blunted cone forebody shapes, an inherent static stability occurs for a centre-of-gravity location of about 40% body length at Mach number above around 1.6, 1.8 and 2 respectively. Such a centre-of-gravity location may not be difficult to achieve with a projectile.

## 4.2. Effect of afterbody

### Zero-lift drag $C_{D0}$

For the projectile configuration comprising conical forebody and boattail, the effect of boattail shape on the drag is shown in Fig. 5(a) as a function of Mach number. For all the investigated configurations, the zero-lift drag coefficient, decreases as Mach number increases. This is a typical behaviour for this curve for all bodies flying at supersonic speeds. The high drag for the cone-cylinder combination was primarily a result of higher base drag than the bodies with boattail. It is also seen from this figure that the higher the angle of boattail the lower is the drag.

### Normal-force-curve-slope $C_{N\alpha}$ and location of centre-of-pressure $x_{cp}$

The effect of afterbody shape on the normal-force-curve slope and centre-of-pressure location for conical nose are shown in Figs. 5(b) and (c) as a function of Mach number. The variations with Mach number are reasonably similar with the most forward location of  $x_{cp}$  occurring with the boattail. The increasing of the angle of boattail results in decreasing of the projectiles static stability.

Accordingly the projectile with cone-cylinder is statically stable above the entire Mach number range, while the projectile with boattail ( $4^\circ$ ) is stable above Mach number 1.8. The cone-cylinder boattail ( $8^\circ$ ) projectile is shown to be stable only within the Mach number range 2 to 4.

## 5. Conclusions

An investigation has been made of the effects of forebody and afterbody shapes of a series of projectiles on the aerodynamic characteristics at Mach numbers from 1.6 to 5. This is done using analytical methods combined with semi-empirical design curves. Some concluding observations from the investigation are given below.

- A pointed cone-cylinder produced the lowest drag at the considered Mach number range, and the highest drag was produced by the blunted cone-cylinder.
- The shape of forebody slightly affects the normal force and centre-of-pressure location. The farthest aft centre-of-pressure locations were obtained with the ogive-cylinder and the most forward locations with a boattailed afterbody.
- With the exception of the boattail afterbody, all the considered projectile shapes indicated inherent static stability above a Mach number of about 2 with the centre-of-gravity location of about 40% body length.
- Configurations with boattail have higher wave drag but appreciably lower base drag with a resultant decrease of total drag. The decrease of the boattail angle increases the base drag but reduced the projectile wave drag with a resultant decrease of the total drag.

## References

1. Vukelich, S.R. and Jenkins, J.E. (1982). Evaluation of component buildup methods for missile aerodynamic prediction. *Journal of Spacecraft and Rocket*, 19(6), 481-488.
2. Shahbhang, V.V. and Rao, R.U. (1970). Normal force characteristics of cone-cylinder & ogive-cylinder bodies at Mach number 1.8. Technical memorandum No. TM-PR.235/69-70, National aeronautical laboratory, Bangalore.
3. Clement, J.W. and deMoraes, C.A. (1951). Results of flight tests to determine drag of parabolic and cone-cylinder bodies of very large fineness ratios at supersonic speeds. *NACA research memorandum*, RML51E18.
4. Cohen, R.J. (1951). Aerodynamic characteristics of four bodies of revolution showing some effects of afterbody shape and fineness ratio at free-stream Mach numbers from 1.5 to 1.99. *NACA research memorandum*, RME51C06.
5. Lebedev, A.A. and Chernobrovkin, L.S. (1973). *Dinamika poleta bezpilotnykh letatelykh apparatov*. "Flight dynamics of unmanned vehicles". Mashinostroenie, Moscow.
6. Jankovic, S. (1979). *Aerodynamika Projektila*. "Aerodynamics of Projectiles" Masinski Fakultet, Univerziteta u Beogradu, Belgrade.
7. Krasnov, N.F. *Aerodynamics. Part 2 (Methods of Aerodynamic Calculations)*. Translated from the Russian Language by G. Leib, Mir Publisher, Moscow (1985).
8. Hoerner, S.F. (1965). *Fluid-Dynamic Drag*. Horner Fluid Dynamics, Brick Town N. J.
9. Mahdi, A. Sh. (2005). *The influence of Configuration Design on the Aerodynamics and Stability of SSM at Supersonic Speeds*. Ph.D. Thesis. Al-Rasheed College of Engineering and Science, University of Technology, Baghdad, Iraq.
10. Brebner, G.G. (1971). A Brief Review of Air Flight Weapons. AGARD Lectures No. 98 'Missile Aerodynamics', NATO. Aerodynamics Department, Royal Aircraft Establishment. Farnborough, Hants GU14 6TD, UK.

## Appendix A

### Representation and Figures of Design Charts

In the present work a number of empirical and semi-empirical design charts are used for the prediction of the aerodynamic characteristics (Figs. A-1 to A-13). These figures are adapted from the design charts given by Lebedev et al [5] and Jankovic [6]. The curves of those charts are read and converted to numerical data and then stored in a separated subroutine in a computer programme described by Mahdi [9]. A simple linear interpolation is used to find the value of the parameters used in the calculations.

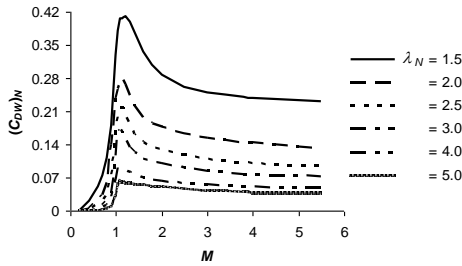


Fig. A-1. Wave Drag Coefficient of Conical Noses with Different Fineness Ratios [5].

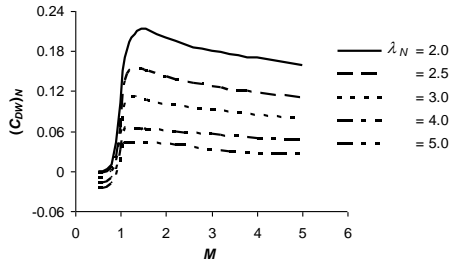


Fig. A-2. Wave Drag Coefficient of Ogival Noses with Different Fineness Ratios [5].

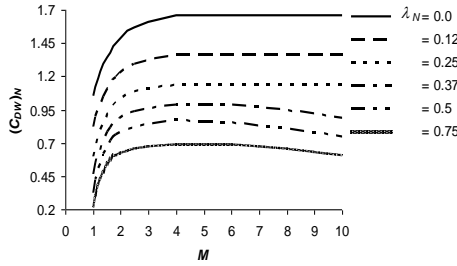


Fig. A-3. Wave Drag Coefficient of Semi-spherical Noses with Different Fineness Ratios [5].

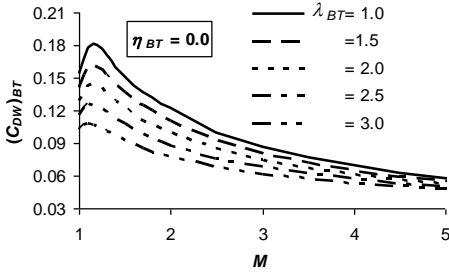


Fig. A-4. Wave Drag Coefficient of Conical Boattails with Different Fineness Ratios (a)  $\eta_{BT}=0.0$ .

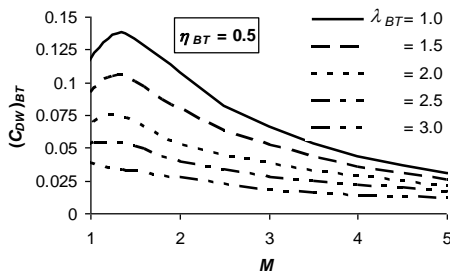


Fig. A-4. Wave Drag Coefficient of Conical Boattails with Different Fineness Ratios (b)  $\eta_{BT}=0.5$ .

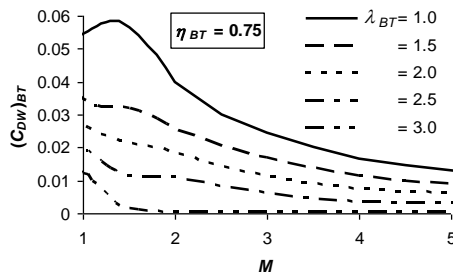


Fig. A-4. Wave Drag Coefficient of Conical Boattails with Different Fineness Ratios (c)  $\eta_{BT}=0.75$ . [5]

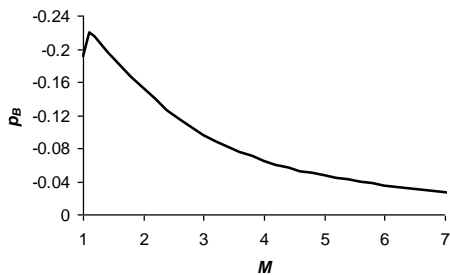


Fig. A-5. Base Pressure Coefficient of Cylindrical Afterbodies [6].

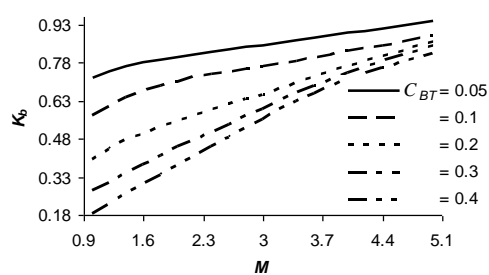


Fig. A-6. Effect of Mach Number and Shape of Boattail on Base Pressure Coefficient [6].

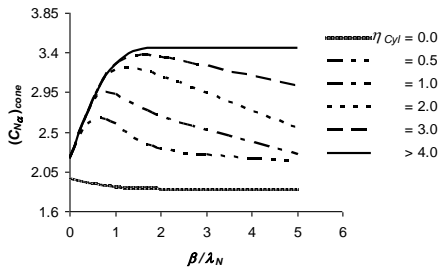


Fig. A-7. Normal Force Curve Slope of Cone-Cylinder Bodies [6].

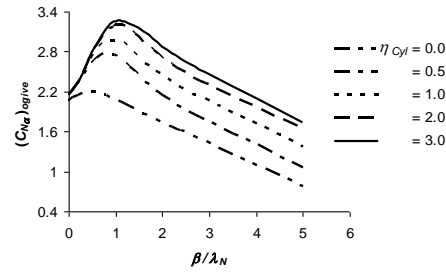


Fig. A-8. Normal Force Curve Slope of Ogive-Cylinder Bodies [6].

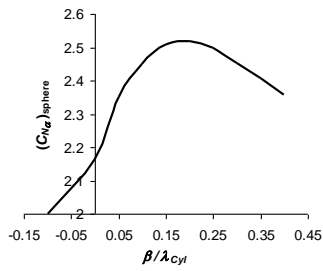


Fig. A-9. Normal Force Curve Slope of Hemi-sphere-Cylinder Bodies [5].

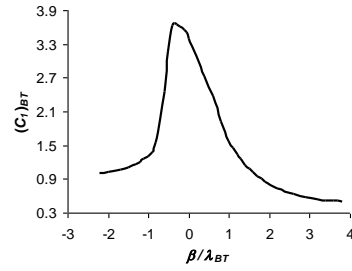


Fig. A-10. Theoretical Normal Force Slope Parameter of Boattail [6].

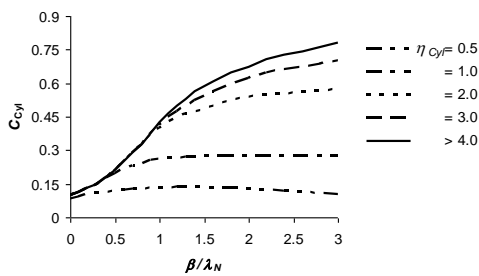


Fig. A-11. Cylindrical Part Effect on Nose Centre of Pressure Coefficient [6].

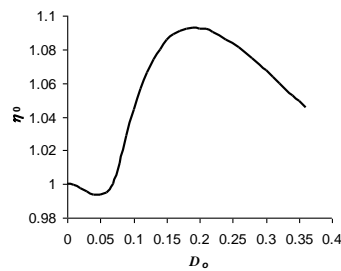


Fig. A-12. Effect of Nose Bluntness on Pressure Coefficient of Forebodies [6].

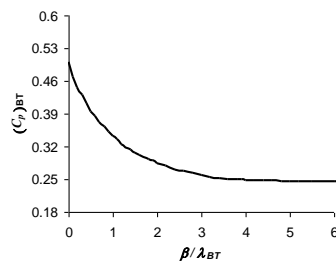


Fig. A-13. Centre-of-Pressure Coefficient for Boattails [6].

## *Appendix B*

### Computer Programme

#### B.1. Introduction

A computer code, for the prediction of projectile aerodynamic characteristics as a function of projectile geometry, Mach number and altitude of flight, is developed in the present work. This programme is based on the analytical and semi-empirical methods presented in section 2.

The computer programme can serve two main purposes: firstly, in the design stage, a rapid parametric study of configuration can be performed to allow the optimum configuration compatible with the requirements to be found and secondly, by calculating the forces acting on a projectile at a range of speeds, the programme is used in conjunction with both trajectory and stability calculations to provide a complete picture of the projectile over its whole flight.

#### B.2. Programme Capabilities and Restrictions

The projectile configurations and flight conditions, which may be analysed by the developed programme, have to meet the restrictions listed in Table B-1.

**Table B-1 Programme Capabilities and Restrictions.**

<b>Projectile Geometry</b>	
Nose Section	Pointed cone, Pointed tangent ogive, Blunted cone
Mid-section	Cylinder with constant diameter and varying length
Tail Section	Cylindrical base, Conical boattail
<b>Flight Conditions</b>	
Mach number	From 1.2 to 4.5
Angle of attack	Zero or small (up to stall)
Altitude of Flight	From 0 to 52 km

#### B.3. Programme Structure and Description of Subroutines

Fortran-77 language is used in programming the prediction methods. Each estimation method is programmed in a separate subroutine for case of modification or addition to the programme. Many of design charts are used in this programme. These charts are converted to numerical data (*Appendix A*) and stored in a separate subroutine for convenience. The main flow chart of the programme is shown in Fig. B-1 and the main two subroutine flow charts are shown in Figs. B-2 and B-3.

As shown from Fig. B-1 the programme firstly reads the input data, which include projectile geometry, dimensions and flight conditions. Then the geometrical parameters of body independent of Mach number are calculated. This considerably reduces the computation time. In the next step the air properties for a given altitude of flight are calculated. The Mach number loop then begins and drag coefficient (Fig. B-1), normal-force-curve slope and centre-of-pressure location (Fig. B-2) are calculated. Final step is the printing of output results as a function of Mach number.

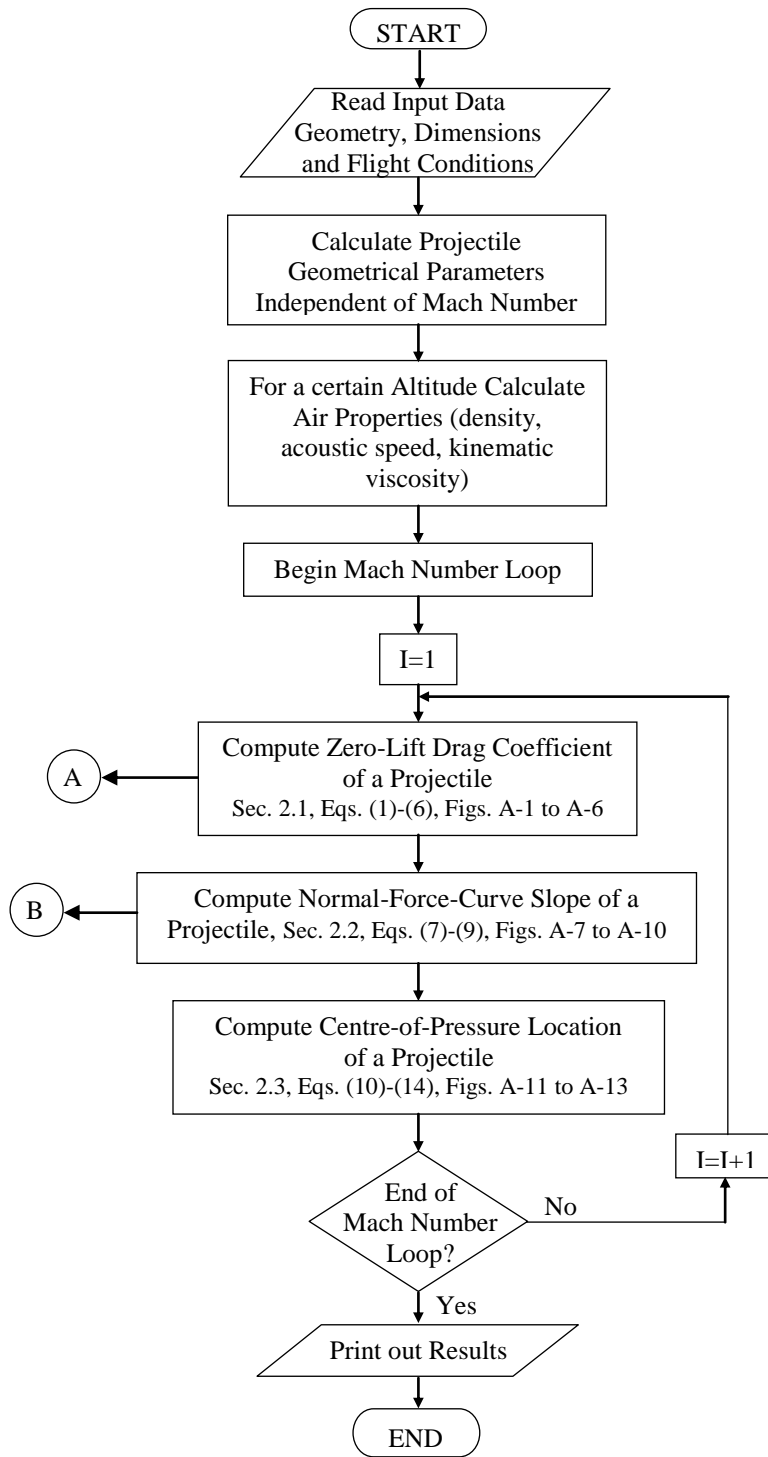


**Fig. B-1 Main Flow Chart of the Computer Programme used in this Study.**

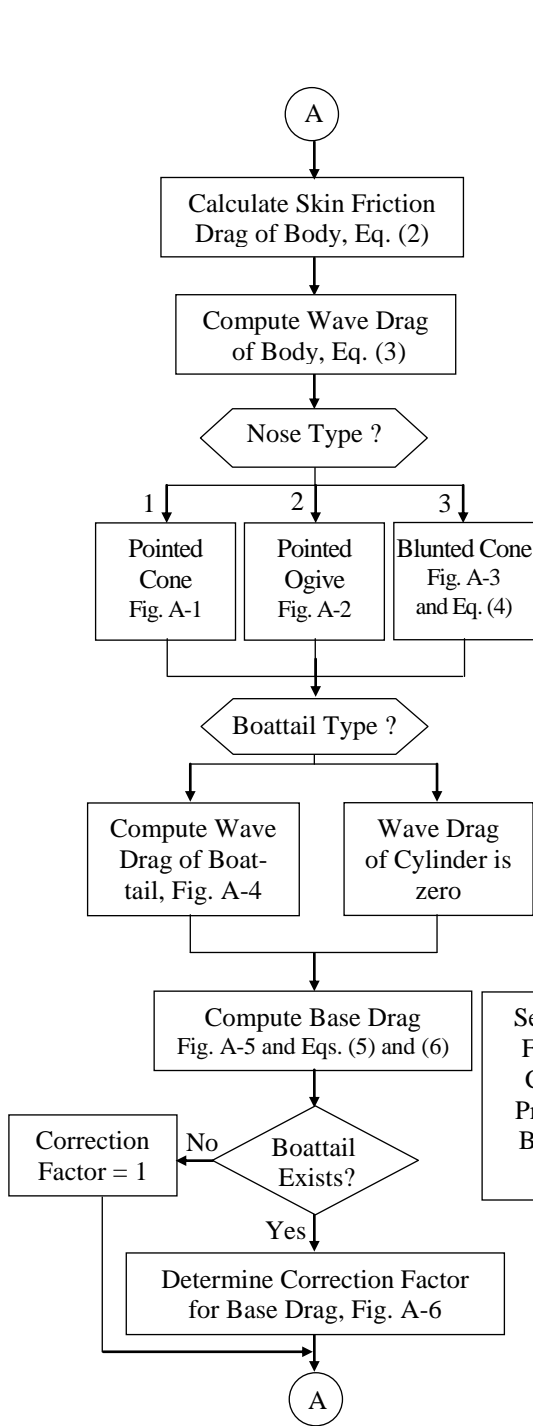


**Fig. B-2 Zero-Lift Drag Coefficient Flow Chart.**

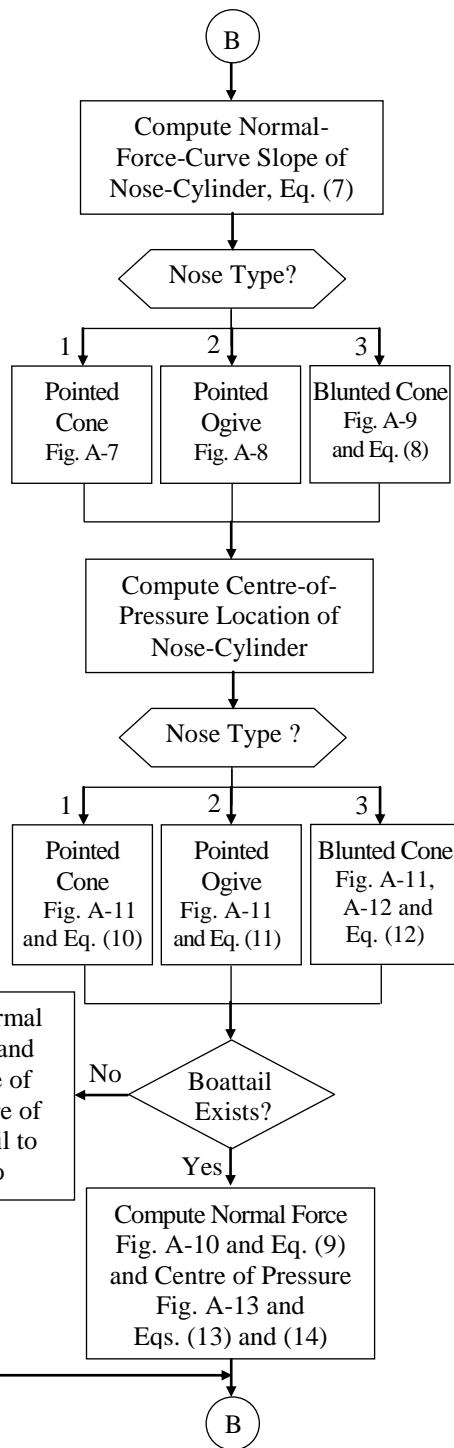


**Fig. B-3 Normal-Force-Curve Slope and Centre-of-Pressure Location Flow Chart.**